colloids and interfaces

MDPI

Article

Optimization and Antibacterial Response of *N*-Halamine Coatings Based on Polydopamine

Nadia Nazi [1,2], Adeline Marguier [3], Catherine Debiemme-Chouvy [2,*] and Vincent Humblot [1,3,*]

[1] Sorbonne Université, CNRS, Laboratoire de Réactivité de Surface, LRS, UMR 7197, 4 Place Jussieu, 75005 Paris, France; nadouche270@gmail.com
[2] Sorbonne Université, CNRS, Laboratoire Interfaces et Systèmes Electrochimiques, LISE, UMR 8235, 4 Place Jussieu, 75005 Paris, France
[3] Institut FEMTO-ST UMR CNRS 6174, Université Bourgogne Franche-Comté, 15B Avenue des Montboucons, 25030 Besançon, France; marguier.adeline@gmail.com
* Correspondence: catherine.debiemme-chouvy@sorbonne-universite.fr (C.D.-C.); vincent.humblot@femto-st.fr (V.H.)

Abstract: Due to the ability of microorganisms to first adhere to a material surface and then to lead to the formation of a biofilm, it is essential to develop surfaces that have antimicrobial properties. It is well known that *N*-halamine coatings allow us to prevent or minimize such phenomena. In the present work, various polydopamine (PDA) coatings containing chloramine functions were studied. In fact, three PDA-based films were formed by the simple immersion of a gold substrate in a dopamine solution, either at pH 8 in the presence or not of polyethyleneimine (PEI), or at pH 5 in the presence of periodate as an oxidant. These films were characterized by polarization modulation reflection absorption infrared spectroscopy and X-ray photoelectron spectroscopy analyses, and by scanning electron microscopy observations. The chlorination of these PDA films was performed by their immersion in a sodium hypochlorite aqueous solution, in order to immobilize Cl(+I) into the (co)polymers (PDA or PDA–PEI). Finally, antibacterial assays towards the Gram-negative bacteria *Escherichia coli* (*E. coli*) and the Gram-positive bacteria *Staphylococcus epidermidis* (*S. epidermidis*) were conducted to compare the bactericidal properties of these three *N*-halamine coatings. Regardless of the bacteria tested, the PDA coating with the best antibacterial properties is the coating obtained using periodate.

Keywords: polydopamine coating; *N*-halamine; antibacterial surfaces; XPS; PM-RAIRS; microbiological tests

Citation: Nazi, N.; Marguier, A.; Debiemme-Chouvy, C.; Humblot, V. Optimization and Antibacterial Response of *N*-Halamine Coatings Based on Polydopamine. *Colloids Interfaces* **2022**, *6*, 9. https://doi.org/10.3390/colloids6010009

Academic Editor: Younjin Min

Received: 29 December 2021
Accepted: 18 January 2022
Published: 28 January 2022

1. Introduction

The fight against the adhesion and proliferation of bacteria on surfaces is a constant concern and a major medical and socioeconomic issue for our society. In the medical and food industries, the bacterial contamination of surfaces is responsible for many nosocomial and food infections through, among other things, prostheses, in operating theaters, in water pipe circuits, or even in food industry installations [1–5]. In addition, this biocontamination of surfaces may also lead to deterioration of the structural and functional properties of the materials, affecting the hulls of ships, as well as civil engineering works, or even cultural heritage [1,6]. Treatments to fight against the biocontamination of materials generate a significant economic impact and are sometimes ineffective, the biofilm lifestyle indeed conferring great resistance to microorganisms [7]. Thus, the prevention of bacterial adhesion appears to be essential and results in the development of antibacterial coatings, as evidenced by the numerous research projects aimed at the development of such systems. One can cite surface functionalization with various antimicrobial molecules, such as enzymes, peptides, organic compounds (aldehyde and quaternary ammonium), or even oxide protective layers [8–12]. Three main classes of antibacterial coatings can be designed in such a

way, either to limit bacterial adhesion, which is called an antiadhesive coating and/or to inhibit the development of bacteria, which are said to be bacteriostatic films, or even to kill bacteria, known as biocidal coatings [13]. These can act by the contact and/or release of antibacterial substances. Quaternary ammonium salts, silver ions or antibiotics are most often found in the literature as biocidal substances incorporated or deposited on matrices, often polymeric, or chemically grafted on surfaces [14–18]. However, the increased resistance of microorganisms to these substances, the surrounding toxicity of these products, and the complexity of grafting or deposition are obstacles to large-scale industrial use. Bio-based compounds, such as enzymes or antimicrobial peptides, have been considered as alternative routes, but their high cost of production and purification, as well as their relative instability in the face of variations in pH or temperature, restrict their use [19–23].

As alternatives to these compounds, a class of antibacterial compounds, *N*-halamines, has attracted great interest in recent years [24–26]. These compounds contain nitrogen–halogen covalent bonds, which are formed by the halogenation of imide, amide or amine groups. The antimicrobial properties of *N*-halamine compounds are due to the halogen, which is in the oxidation state (+I) and which, therefore, has oxidizing properties. It can react with suitable biological receptors, such as the thiol groups of amino acids within bacteria. This reaction can interfere with the metabolism of cells, such as respiration, especially protein-related processes, resulting in the death of the bacteria [24]. The disinfectant effectiveness of *N*-halamines is similar to that of bleach (sodium hypochlorite), but these compounds are more stable, less corrosive, and relatively easy to generate. Indeed, after the immobilization of the precursors (containing the following NH groups: primary or secondary amine, amide or imide) of *N*-halamine on a surface, they are converted into haloamine functions by a halogenation process (substitution reaction of H by Cl(+I) or Br(+I)), thanks to a sodium hypochlorite or a sodium hypobromite solution, to generate chloramine or bromamine functions, respectively [24,25,27].

Various methods for bonding *N*-halamines to substrate surfaces have been described; however, these methods often require either complex surface pretreatment or lengthy coating formation procedures, and often lack universality, with the strategies employed being specific to the physical and chemical properties of the surfaces of materials. In this context, polydopamine (PDA), an aqueous insoluble biopolymer produced by the 'auto-oxidation' of a catecholamine neurotransmitter, dopamine (DA), has become a highly studied polymer in materials science as a functional bio-system, used in a very wide range of applications. PDA provides exceptional adhesion properties, producing a universal coating and offering the possibility of a large repertoire of post-functionalization, which has paved the way for many applications in biomedical sciences and in the process of energy conversion or water treatment devices [28,29].

In a previous study, we demonstrated that it is possible to elaborate a new antibacterial coating, formed by a thin chlorinated PDA film [26]. This film is obtained by dopamine monomer polymerization in mild basic aqueous solutions, followed by treatment in sodium hypochlorite (NaOCl) solution. This treatment leads to the formation of chloramine functions inside the polymer, estimated to be between 10^{21} and 10^{22} at·cm^{-3} [26]. Microbiological tests towards *Escherichia coli* (*E. coli*) bacteria showed that chlorinated PDA coatings reduced *E. coli* adhesion by up to 45% compared to uncoated surfaces, while, at the same time, bacterial viability was reduced by 34% with a chlorinated PDA coating compared to initial PDA films.

However, the maximum thickness obtained for the deposition of PDA in alkaline conditions, in the presence of O_2 as an oxidizing agent, is less than 50 nm, which hinders any optimization of the antibacterial effect of the coating by increasing the thickness of the deposit, in order to maximize the number of amine functions available. Moreover, many materials or molecules sensitive to pH, such as cellulose, polyester, phenolic resins, proteins or certain gels, are not suitable for functionalization by dopamine in an alkaline

aqueous medium. In short, the fabricated PDA films are unstable in a strong alkaline environment [30–32].

To address these issues, various ways of optimizing the coating were considered during this study. First of all, one could increase the thickness of the PDA film by modifying the oxidant, replacing O_2 with sodium periodate, which allows (i) deposition in an acidic medium with faster kinetics and (ii) for thicker films to be obtained [32]. The second path explored is based on the introduction of more amine functions through polyethyleneimine (PEI), forming a PDA–PEI composite. Moreover, amino-rich PEI has been frequently introduced as a cross-linking agent, which affords free-standing PDA–PEI composite films by Michael addition or Schiff base reaction, and improves the chemical stability in a strong alkaline environment [33]. *N*-halamine based on the co-deposition of PDA and PEI was studied, and it was shown that the antibacterial ability of the coatings increased as the PEI content increased. In addition, the chlorinated co-deposition coatings had significantly increased antibacterial properties compared to the non-chlorinated coatings, with the chlorinated co-deposition coatings inactivating >99.99% of *Staphylococcus aureus (S. aureus)* and >99.9% of *E. coli* after contact for less than 10 min with PDA antibacterial materials [27,34].

Thus, in the present work, the optimization of the synthesis of a PDA coating containing chloramine functions was studied. For this purpose, first, the formation of three PDA-based films on a gold surface was performed by simple immersion of the substrate in a dopamine solution, either at pH 8.5 in the presence or not of PEI, or in a dopamine solution in the presence of sodium periodate as an oxidizing agent at pH 5. These films were characterized by polarization modulation reflection absorption infrared spectroscopy (PM-RAIRS) and X-ray photoelectron spectroscopy (XPS) analyses, and by scanning electron microscopy (SEM) observations. The chlorination of the PDA films was performed by immersion in a NaOCl aqueous solution, in order to immobilize Cl(+I) oxidative species into the polymers. Finally, antibacterial assays against *E. coli* and *Staphylococcus epidermidis* (*S. epidermidis*) were conducted to compare the bactericidal properties of the *N*-halamine coatings.

2. Materials and Methods

Dopamine hydrochloride (98% purity), branched PEI (average M_W ~800 g·mol^{-1} by light scattering, average Mn ~600 motifs by gel permeation chromatography), sodium periodate (99.8% purity), tris-(hydroxylmethyl)aminomethane hydrochloride (Tris-HCl), sodium acetate (99% purity), and phosphate buffer saline (PBS) were obtained from Sigma-Aldrich (St-Quentin Fallavier, France). A household bleach solution with 2.6% of active chlorine was diluted before being used for the chlorination of the PDA films. Ultrapure water was obtained from a Milli-Q system (Millipore, resistivity of >18 MΩ·cm^{-1}) from EMD Millipore Corp. (Billerica, MA, USA).

Glass substrates (11 mm × 11 mm), coated with a 5-nm-thick layer of chromium and a 200-nm-thick layer of gold, were purchased from Arrandee (Werther, Germany). Before PDA coating, the gold-coated substrates were annealed in a butane flame to obtain a crystal reconstruction of the first atomic layers, and a 15 min UV−ozone cleaning procedure was then applied, prior to ultrapure water and absolute ethanol rinsing for a period of 10 min each [35].

2.1. PDA Coatings

2.1.1. PDA–O_2

For the formation of the PDA coating, the substrates were immersed in a dopamine solution, prepared by dissolving 0.5 mg mL^{-1} of dopamine in 10 mM of Tris at pH 8.5. This PDA film deposition protocol was inspired by the protocol proposed by the Messersmith group [36,37]. Then, ultrasonic rinsing treatment in distilled water was carried out on the substrates for 1 min. Finally, the samples were dried with dry nitrogen. The samples were subsequently named PDA–O_2.

2.1.2. PDA–IO_4^-

For the deposition of PDA using sodium periodate ($NaIO_4$) as an oxidant at a concentration of 5 mM, the substrates were immersed in dopamine solution, prepared by dissolving 0.5 mg mL^{-1} of hydrochloric dopamine in 50 mM sodium acetate at pH 5.5. This protocol was inspired by the study conducted by Ponzio et al. [32]. Subsequently, the substrates were washed with ultrapure water for 5 min under sonication and then dried with dry nitrogen. The samples were subsequently named PDA–IO_4^-.

2.1.3. PDA–PEI

The deposition of the PDA–PEI composite was carried out by immersing the substrates in a solution formed from a mixture of dopamine at 0.5 mg mL^{-1} and PEI at 0.25 mg mL^{-1} in 10 mM of Tris at pH 8.5, under stirring. This PDA–PEI composite film deposition protocol was inspired by the study conducted by Xu et al. [33]. This functionalization is followed by ultrasonic treatment of the substrates in ultrapure water and followed by drying with dry nitrogen. The samples were subsequently named PDA–PEI.

2.2. PDA Film Chlorination

For chlorination, PDA–XX films were soaked in 1 or 10 mM NaOCl solution at pH 10, at room temperature [26,38,39]. After chlorination, the substrates were thoroughly washed with deionized water and nitrogen dried. After chlorination, the coatings were named PDA–XX–Cl.

2.3. Polarization Modulation Reflection Absorptions InfraRed Spectroscopy (PM-RAIRS)

PM-RAIRS measurements were carried out on a Nicolet Nexus 5700 Fourier-transform infrared (FT-IR) spectrometer (Madison, WI, USA) equipped with a wide-band HgCdTe detector cooled with liquid nitrogen. Infrared spectra were obtained by addition of 128 scans at 8 cm^{-1} resolution. A ZnSe photoelastic modulator and a ZnSe grid polarizer were placed prior to the sample to modulate the incident beam between p and s polarizations (PM90, HINDS Instruments, Inc., Hillsboro, OR, USA), with a modulation frequency of 36 kHz. Interferograms (sum and difference) were processed via Fourier transformation to obtain the resulting PM-RAIRS signal, which is the differential reflectivity, as shown below:

$$\Delta R/R^0 = (Rp - Rs)/(Rp + Rs) \quad (1)$$

where R^0 is the reflectivity of the initial IR beam and R is the reflectivity after reflection on the substrate; Rs and Rp are the signals perpendicular and parallel to the incident plane, respectively.

2.4. X-ray Photoelectron Spectroscopy (XPS)

XPS analyses were performed using an Omicron Argus spectrometer (Taunusstein, Germany) equipped with a monochromated Al Kα X-ray source (hν = 1486.6 eV) working at an electron beam power of 300 W. Photoelectron emission was analyzed at a take-off angle of 45°. The analyses were carried out under ultrahigh vacuum conditions ($\leq 10^{-10}$ Torr) after introduction via a load lock into the main chamber. Spectra were obtained by setting up a 100 eV pass energy for the survey spectra, and a pass energy of 20 eV was chosen for the high-resolution regions. Element peak intensities were corrected by Scofield factors [40]. CasaXPS software (Casa Software Ltd., Teignmouth, UK) was used to decompose XPS spectra using a Gaussian/Lorentzian ratio of 70/30.

2.5. Water Contact Angle (WCA)

Static water contact angles (DSA100 apparatus, Krüss, Hamburg, Germany) were measured under ambient conditions (at 20 °C and 40% relative humidity) by analyzing the profile of sessile drops (1 µL droplet of Milli-Q water) deposited on a given surface. The drop profile was recorded by a CCD camera, while the angles were measured by the

image analysis software. For each analyzed surface, at least four different locations were chosen for the deposition of the droplet; each test was performed in triplicate on three different samples. The reported values for a given surface are thus the averages of these 36 measurements.

2.6. Chemical 5-Thio-2-nitrobenzoic Acid (TNB) Titration

The presence of chloramine functions was confirmed by measuring the bleaching of a 5-thio-2-nitrobenzoic acid (TNB) solution at 412 nm [41]. Fresh TNB solution was produced before each experiment via addition of 2 equivalents of cysteine (Cys) to 1 equivalent of 5,5′-dithiobis(2-nitrobenzoic acid) (DTNB) following the reaction, as shown below:

$$\text{DTNB} + 2\,\text{Cys} \rightarrow 2\,\text{TNB} + \text{cystine} \quad (2)$$

For this aim, in equal volumes, 2×10^{-3} M cysteine and 10^{-3} M DTNB were mixed in 50 mM phosphate buffer solution (PBS) at pH 7.4, giving a highly colored yellow/orange solution [42]. Then, this stock solution was diluted 10-fold with 50 mM PBS, pH 7.4. The different substrates were immersed in this solution for 24 h. The yellow-colored TNB reacts with haloamine functions to regenerate colorless DTNB. The UV/visible absorbance measurements were carried out using a spectrometer with 1 cm path length cuvettes. According to Beer−Lambert's law, the density of chloramine functions (d_{Cl}), in at cm^{-3}, was calculated according to the following equation:

$$d_{Cl} = \frac{A_{PDA} - A_{PDA-Cl}}{2\,\varepsilon\,l\,V_{coating}}\,V_{TNB}\,N_A \quad (3)$$

where A_{PDA} and A_{PDA-Cl} are the absorbance of the TNB solution containing the substrate with the PDA coating and with the chlorinated PDA coating, respectively, ε is the molar extinction coefficient of TNB, ε = 14,100 M^{-1} cm^{-1}, l is the length of the light path, l = 1 cm, $V_{coating}$ is the volume of the PDA film in cm^3, V_{TNB} is the volume of the TNB solution in L and N_A is Avogadro's constant.

2.7. Microbiological Tests

Microbiological experiments were conducted with *Escherichia coli* ATCC 25922 described as a rod shape with an average height of 1 µm and *Staphylococcus epidermidis* CIP 6821 described as a sphere ranging from 1 to 2 µm in diameter. *S. epidermidis* strain was chosen as non-pathogenic bacteria mimicking *S. aureus* bacteria. The following three culture media were used for these experiments: 2 nutritive media, Lysogeny Broth medium (LB) for *E. coli*, Mueller−Hinton medium (MH) (Sigma-Aldrich, St-Quentin Fallavier, France) for *S. epidermidis* and a nonnutritive phosphate buffer saline (PBS) medium for killing experiments.

Bacteria were stored at −80 °C. Before the tests, they were incubated overnight on LB agar plate for *E. coli* and MH agar plate for *S. epidermidis*, at 37 °C. Then, a liquid pre-culture was prepared with one colony of *E. coli* or *S. epidermidis* in LB or MH media, respectively, and incubated for 18 h at 37 °C under stirring (90 rpm). Bacteria were then harvested by centrifugation (3500 rpm, 4 °C, 20 min). Bacteria were re-suspended in the PBS medium and bacterial suspensions were adjusted to an absorbance at 620 nm of 0.01 (5×10^6 CFU mL^{-1}).

2.7.1. Bacteria Growth Capacity (Cultivability of Adhered Bacteria)

Bacterial growth capacity after contact with functionalized surfaces was determined by performing killing tests. Before bacterial inoculation, the surfaces were disinfected by washing them five times with ethanol solution at 70%. The killing test was performed in sandwich configuration. For this, 20 µL of the bacterial suspension in PBS media was deposited on the first plate; then, a second plate was placed onto the first one, on the coating side so that the bacterial suspension was sandwiched between the two substrates. After 3 h

of contact, at room temperature, the surfaces were mildly rinsed with sterile PBS in order to remove non-adhered bacteria, then transferred into a tube containing 2 mL of sterile PBS solution and sonicated (Bandel in Sonorex RK 31, Berlin, Germany; f = 35 kHz and P = 90 W) for 2 min to recover the adhered bacteria without damaging them. After sonication, SEM observations of the plates were performed to verify that most of the adhered bacteria were detached during the sonication process. Traditional dilution/counting was carried out in triplicate on LB or MH agar plates. The plates were incubated at 37 °C overnight before enumeration. Results were expressed in the number of attached and cultivable bacterial cells onto the different surfaces per mL (CFU·mL^{-1}). The percentage of killing (*%killing*) was calculated using Equation (4), as follows:

$$\%killing = 100\ (CFU_{ref} - CFU_{chlorinated\ surface})/CFU_{ref} \quad (4)$$

Each test was performed in triplicate and the number of CFU·mL^{-1} is the average of the results obtained for each sample.

2.7.2. Epifluorescence Optical Microscopy Observations

Samples were immersed in 4 mL of bacterial suspension and incubated for 3 h at 37 °C. It is important to keep in mind that this incubation time corresponds to the limit of the reversible phase in the biofilm formation process. Surfaces were then thoroughly and carefully rinsed 8 times by replacing 1 mL of the bacterial suspension with 1 mL of fresh PBS solution to remove non-attached bacteria. Adhered bacteria on the surfaces were fluorescently stained by adding 1 µL of 5×10^{-3} M SYTO9® (Invitrogen, Waltham, MA, USA) solution and 3 µL of 5×10^{-3} M Propidium Iodide® (Invitrogen, Waltham, MA, USA) solution and were incubated for 15 min at 37 °C.

Then, the surfaces were directly observed in the last rinsing solution by using the fluorescence/reflection mode of an upright epifluorescence microscope (Axio Observer, Zeiss) equipped with a long working distance water objective (W Plan-Apochromat 63X/1.0, working distance 2.0 mm, Zeiss®). On each surface, micrographs were taken at 10 random locations. Experiments were conducted with two surfaces of each type and reproduced by 3 independent experiments. Micrographs were analyzed by ImageJ V.1.44d software® (NIH). Each image was processed to select the color channel and adjust thresholds by Otsu or Intermodes method depending on the intensity histogram of each image. Then, the number of adhered bacteria (N) and their size on each micrograph were calculated with the help of the analyze particle plug-in. The *%killing* was calculated using Equation (5), as follows:

$$\%killing = 100\ (N_{green\ +\ red\ bacteria} - N_{red\ bacteria})/N_{green\ +\ red\ bacteria} \quad (5)$$

The significance of two-by-two differences between average cell number in the diverse culture conditions was evaluated by bilateral Student's t tests (application conditions: independent data and equal variances assessed by F-test) with significance thresholds of 0.01 and 0.05. The alternative hypothesis ($\mu_1 \neq \mu_2$) was assumed to be true when the main hypothesis ($\mu_1 = \mu_2$) was rejected, where μ_1 and μ_2 are the average cell numbers (or values) to be tested for significant difference.

3. Results

3.1. PDA Coating Elaboration

In an aerated solution, dopamine monomers are known to self-polymerize upon oxidation within the right concentration and pH conditions. The polymerization is usually accompanied by a change in the solution color, from colorless to dark brown [26]. In this study, we studied several ways of obtaining PDA films by changing the oxidant agent, atmospheric O_2 or sodium periodate, or by adding a small polymer, PEI, which is known as a good reticulate agent [34,43].

DA polymerization was followed by increasing the contact time between the gold substrates and the DA solutions (Figure S1). Figure 1 presents the PM-RAIRS data obtained for the three routes of PDA grafting, showing a similar profile. According to a previous study on the formation of PDA films using atmospheric O_2 as an oxidant [26], in Figure 1a, a broad IR massif is observed in the 1600 cm^{-1} region, with a second group of features visible at lower wavenumbers. These IR features indicate the presence of a PDA film, with the main characteristic peaks observed at 1620 and 1515 cm^{-1}, assigned to the stretching of the C=C group within the DA ring, together with the stretching ν(N−H) vibrations [44], respectively. In the second region, IR peaks are observed at 1450, 1350, and 1290 cm^{-1}, respectively, and assigned to the stretching vibrations (C-N-C) of the DA ring and to the free catechol moieties of free dopamine, ν(C−O) and ν(C=N). These PM-RAIRS features are consistent with the formation of a PDA coating on a gold surface [44–47].

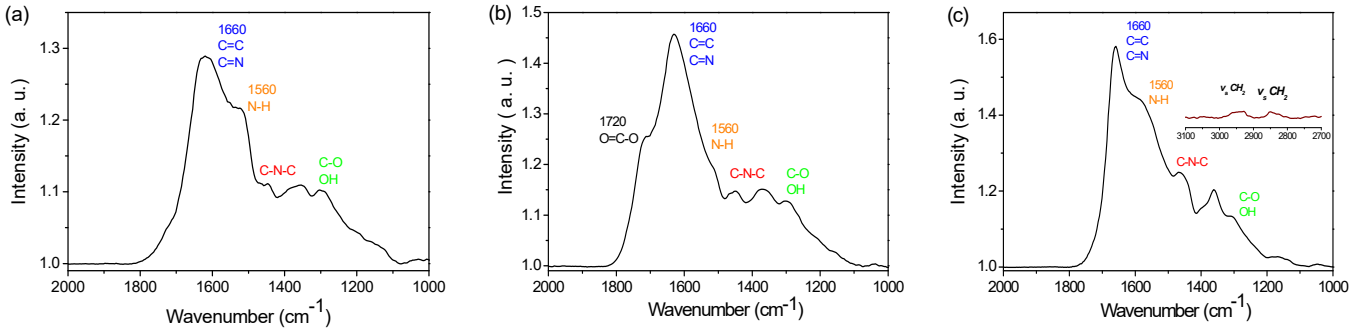

Figure 1. PM-RAIRS spectra of gold surface coated with (**a**) PDA–O_2, (**b**) PDA–IO_4^-, (**c**) PDA–PEI.

PM-RAIRS analyses of the spectrum obtained using sodium periodate are presented in Figure 1b; the spectrum obtained after 5 h revealed the same characteristic groups of PDA observed previously for the PDA–O_2 film at 24 h. However, one can also note that a new peak appears at 1720 cm^{-1}, assigned to the stretching vibration of a C=O bond of a carboxylic group. This peak suggests a hyperoxidized state of the PDA, due to the strong oxidizing power of periodate. The material is probably richer in carboxylic groups or quinonoid structures and has undergone a partial loss of carbon [31]. This is in accordance with the known chemistry of periodate, which, when used in excess, can cause *o*-quinone oxidative cleavage [48]. The spectrum obtained for the PDA–PEI film after 24 h (Figure 1c) is also similar to the spectrum obtained for PDA–O_2. In addition, IR features are also observed in the 2800–2900 cm^{-1} region, assigned to the stretching vibration of CH_2 groups from the PEI backbone. Finally, it is important to note that the intensity of the NH vibration at 1560 cm^{-1}, compared to the C–C and C=N at 1660 cm^{-1}, is greater in the latter case, suggesting the presence of more NH groups in the case of the PDA–PEI film [34].

PDA film growth can be quantitatively investigated using PM-RAIRS data, by integrating the area under the IR features as a function of immersion time (Figure S1), as presented in Figure 2. The growth profiles observed are quite different for all three polymerization routes. For the PDA–O_2 films, a rapid increase in the peak's intensity is observed for the first 12 hours, followed by the slowest increase, which plateaus after 48 h. This stationary phase can be attributed to the depletion of the monomer in the supernatant solution, which is able to crosslink on the PDA film, in favor of non-reactive quinone molecules [49]. The ellipsometry data (Figure S2B) confirm the logarithmic kinetic deposition profile obtained by PM-RAIRS analysis. On the contrary, the PDA–IO_4^- films show an even faster increase in IR intensity during the first 3 to 5 h, which quickly stabilized into a plateau regime. The thickness measurements obtained by SEM (Figures S2A and S3) also confirm the deposition kinetics observed by PM-RAIRS, faster than during conventional deposition. For this, logarithmic kinetics are observed. Finally, the data obtained for the PDA–PEI film seem to be a mix of both previous methods, with a fast increase at 5 h, though smaller than for PDA–IO_4^-, followed by the slowest increase up to a steady-state obtained af-

ter 10 h of immersion. It is important to note that the intensity of the areas under the peaks are expressed in arbitrary units; thus, calibration was applied using the thickness obtained on the plateau regime, using ellipsometry analysis and SEM observations [26] (Figures S2 and S3), showing similar thicknesses for both PDA–O_2 and PDA–PEI, around 50–55 nm and 60–65 nm, respectively, while for PDA–IO_4^-, the film thickness reached 110–115 nm [32]. Thus, one can conclude that periodate has strong efficiency as an oxidant agent compared to atmospheric O_2, leading to a greater thickness of PDA films, together with a faster growth rate. Consequently, the use of periodate allows us to accelerate the oxidation kinetics of dopamine. After 5 h of immersion, a thickness plateau around 100 nm is reached, i.e., a gain of 60 nm in thickness, compared to the conventional deposit obtained after 24 h. Additionally, the copolymerization of PDA and PEI leads to similar thickness of the film to PDA–O_2, with a kinetic growth rate that increased by a factor of two in the case of PDA–PEI, the hypothesis being that there is a greater concentration of NH groups.

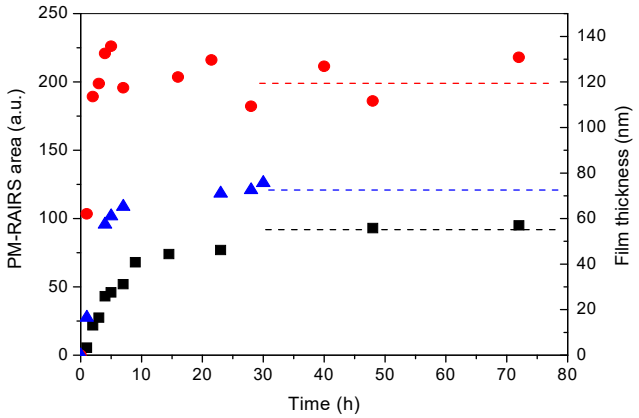

Figure 2. PDA film growth. PM-RAIRS peak area (left axis) and film thickness (right axis) vs. immersion time in DA solution. Data are from Figures S1–S3. Square: PDA–O_2. Circle: PDA–IO_4^-. Triangle: PDA–PEI.

Contact angle measurements with water were used to assess the wettability of a surface and to demonstrate a change in the chemistry of the latter, following surface modification (Figure S4). It is noted that for the PDA–O_2 coating, the contact angle decreases over time to reach a plateau after 3 h of deposition, around 55°, which approaches the value of the contact angle reported in the literature [32]. It can be observed that this monitoring of wettability makes it possible to have, in a simple and rapid way, an indication of the time at the end of which the coating will become homogeneous at the macroscopic level, in terms of coverage of the substrate, and, thus, this completes the monitoring by PM-RAIRS and ellipsometry.

Concerning PDA–IO_4^-, the evolution of the contact angle formed between the coating and the water matches the profile obtained for the PDA–O_2 coating. In fact, a sharp reduction in the angle is observed during the first 10 h, then a plateau is observed, indicating the presence of a homogeneous coating on the gold surface. Note that this change is similar to the profile found when monitoring the thickness of the deposit. Thus, just as with the PDA–O_2 coating, the kinetic monitoring of the deposit by measuring the contact angle is, in fact, a simple method of monitoring the PDA deposit over time. Finally, it is noted that PDA–O_2 and the PDA–PEI composite have the same evolution profile of wettability during the first 30 h of deposition. Indeed, the contact angle with water decreases over time to reach a plateau after 5 h of deposition, around 50°, which is slightly lower than the value obtained for pure PDA.

XPS analyses were performed on these three sets of PDA-coated Au surfaces; the survey spectra are presented in Figure 3. For all the samples, the photopeaks C1s (285 eV), O1s (530 eV), and N1s (400 eV) were observed, whereas the Au4f contribution (84 eV) was not detected, confirming a film thickness greater than 15 nm [50]. In addition, for

PDA–IO_4^-, an I3d signal at 620–630 eV was observed, together with a counter-ion Na^+ signal at 1051 eV. For the samples PDA–O_2 and PDA–IO_4^-, the chemical composition in carbon and nitrogen is close to the theoretical composition of PDA (N/C = 0.125), taking into account the carbon contamination, which slightly reduces the N/C ratio (Table 1). Finally, for the PDA–PEI sample, the atomic percentage of N is much greater than for the two other films, due to the presence of PEI as a copolymer in the film, with the N/C ratio being, accordingly, twice as large as previously.

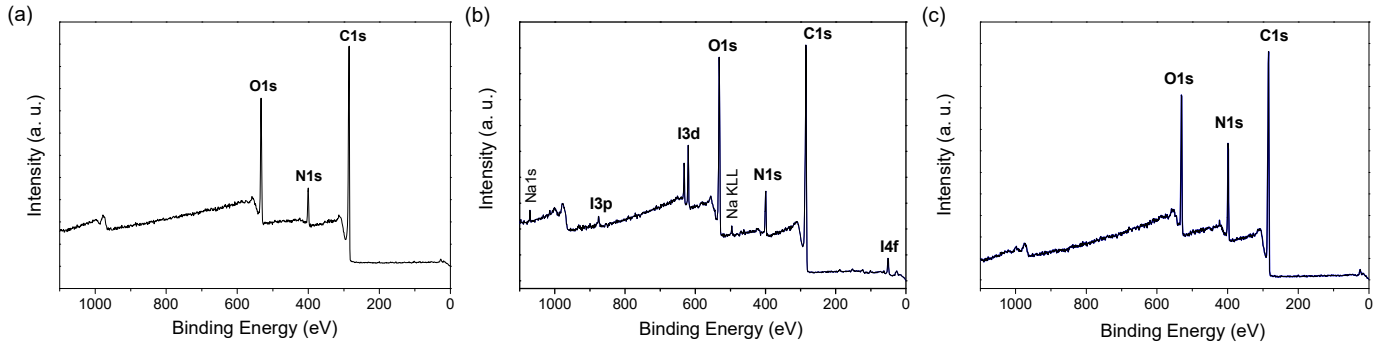

Figure 3. XPS survey spectra of gold surface coated with (**a**) PDA–O_2, (**b**) PDA–IO_4^- and (**c**) PDA–PEI.

Table 1. Atomic percentages and N/C ratio obtained from XPS data.

	C	N	O	Au	I	Na	N/C
PDA–O_2	75.5	7.3	17.2	ND	-	-	0.1
PDA–IO_4^-	72.2	7.1	19.3	ND	0.9	0.5	0.1
PDA–PEI	69.4	15.4	15.2	ND	-	-	0.2

ND = non detectable.

3.2. PDA Coating Chlorination

Chlorination of the different PDA films was carried out using diluted NaOCl as a function of contact time and concentration, in order to optimize the chlorination process. Figure 4 shows the evolution of the PM-RAIRS spectra upon increasing the contact time between the PDA films and the NaOCl solution. Two concentrations of the NaOCl solutions were tested, 1 and 10 mM. After a certain time, drastic changes in the profile spectra were observed, suggesting degradation of the film, as a long contact time with an alkaline solution can degrade the polymer structure [38,51,52]. It is first observed that after chlorination, a change in the IR spectra of the three PDA films was observed. In fact, the latter appears to show a strong decrease in the peak at 1515 cm^{-1}, a peak attributed to the deformation vibration of the δ(N-H) amine bond, therefore suggesting the creation of chloramine functions. There is also a shift in the peak characteristic of the aromatic cycle from 1620 cm^{-1} to 1645 cm^{-1}. This change could be a consequence of the grafting of chlorine atoms on nitrogen atoms, located near the aromatic ring, modifying the chemical environment of the latter. Finally, the appearance of a shoulder at around 1720 cm^{-1}, the intensity of which increased with the chlorination time (Figure 4), may be ascribed to the appearance of carboxylic functions, due to the oxidation of the PDA coating upon contact with hypochlorite ions.

For instance, on the PDA–O_2 films (Figure 4a,d), the intensities of the peaks of the chlorinated spectra started to decrease for a contact time of 15–20 min, with complete destruction of the film after 50 min of contact time with the NaOCl solution. Thus, an optimized contact time for the chlorination process for PDA–O_2 was chosen to be 20 min at 1 mM. The same processes were applied for the PDA–IO_4^- and PDA–PEI films (Figure 4b,c,e,f), resulting in optimized chlorination times of 20 min at 1 mM and 10 min at 10 mM, respectively.

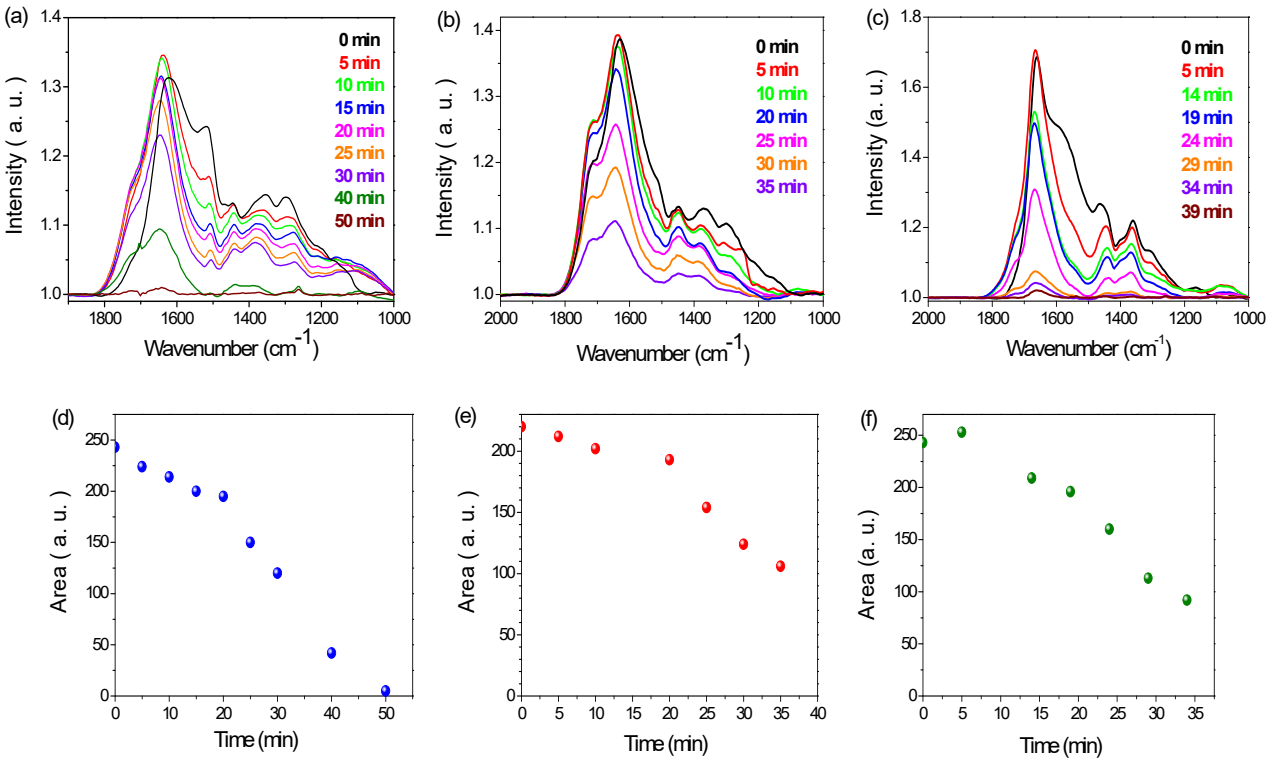

Figure 4. Chlorination of PDA films as a function of immersion time in (**a**,**b**) 1 mM, (**c**) 10 mM NaOCl solution. (**a**–**c**): PM-RAIRS spectra. (**d**–**f**): area under IR peaks. (**a**,**d**): PDA–O_2; (**b**,**e**): PDA–IO_4^-; (**c**,**f**): PDA–PEI.

XPS experiments were carried out for the different PDA films chlorinated with optimized conditions. The data are presented in Figure 5 and the quantitative data are summarized in Table 2.

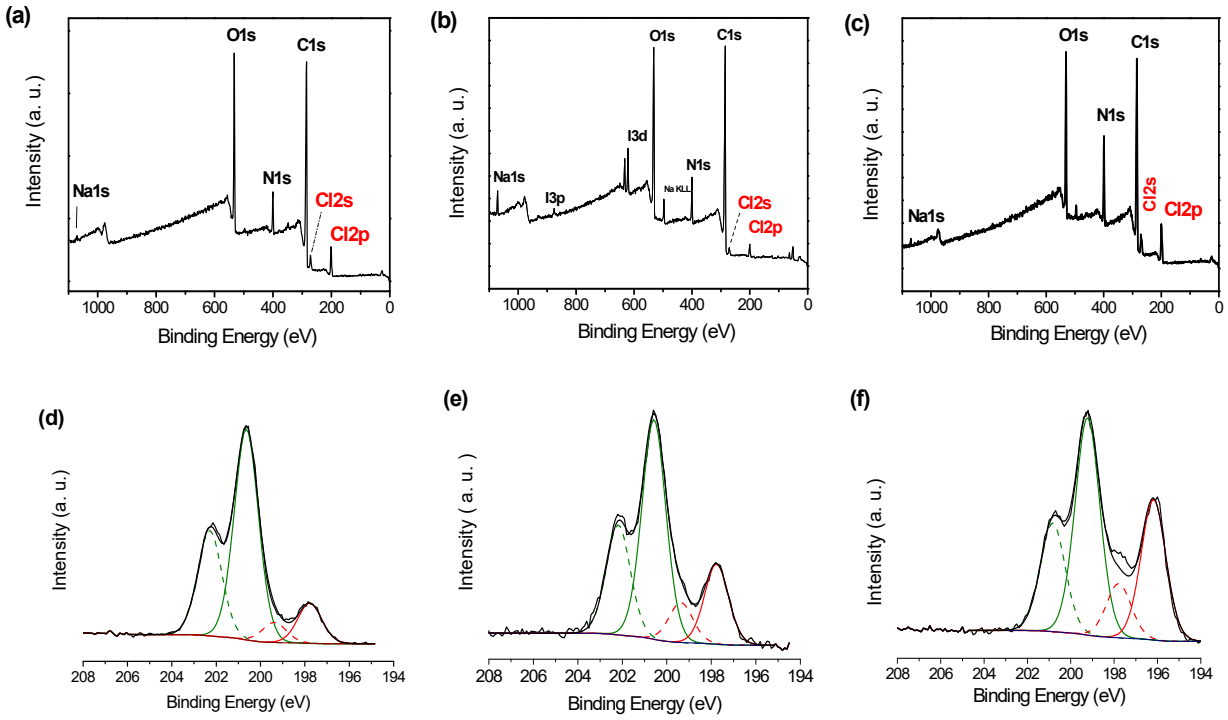

Figure 5. XPS survey spectra (**a**–**c**) and high-resolution Cl2p spectra (**d**–**f**) after chlorination of (**a**,**d**) PDA–O_2, (**b**,**e**) PDA–IO_4^- and (**c**,**f**) PDA–PEI.

Table 2. Atomic percentage and ratio obtained from XPS data for PDA coatings after chlorination.

	C	N	O	I	Au	Na	N/C	Cl_{total}	Cl_{200}	Cl_{200}/N
PDA–O_2–Cl	69.85	6.45	18.9	-	-	-	0.1	4.8	4.0	0.6
PDA–IO_4^-–Cl	69.2	6.5	20.0	0.7	-	1.3	0.1	2.3	1.7	0.3
PDA–PEI–Cl	61.4	13.7	16.4	-	-	0.8	0.2	7.7	4.5	0.3

The survey spectra in Figure 5a–c show additional contributions at 200 eV and 270 eV, assigned to Cl2p and Cl2s contributions, respectively, confirming the successful chlorination of the PDA films. The high-resolution spectra of the Cl2p contribution are also shown in Figure 5d–f, exhibiting two distinct doublets centered for the $Cl2p_{3/2}$ contribution, at around 200 eV and 198 eV. The most intense contribution (plain lines), at 200 eV, named Cl_{200}, is usually assigned to chlorine atoms in the N–Cl bond, while the lower binding energy contribution (dashed lines) is ascribed to free chlorine atoms. Thus, one can first conclude that the chlorination process was successful, and, second, that only a few free Cl atoms remained at the surface, even after the heavy rinsing procedure. It is interesting to note that the amount of Cl_{200} differs from one film to another; thus, both PDA–O_2 and PDA–PEI exhibit N atomic percentages of about 4.0%, while the PDA–IO_4^- film shows only 2.7%. However, per se, such analyses are not sufficient to conclude that one film or another contains the highest amount of haloamine functions. In fact, one should consider the original amount of N1s atoms present in the analyzed thickness of the films, and it is possible to calculate the percentage of chlorinated NH groups by looking at the Cl_{200}/N ratio. From Table 2, it can be concluded that the efficiency of chlorination is the best for the PDA–O_2 film, with more than 60% of the N atoms being chlorinated, while this value is only 30% for the two other PDA films.

These results, thus, only give us information on the composition of the surface of the coating (10–15 nm of thickness probed). These differences between the PDA–O_2, PDA–IO_4^- and PDA–PEI coatings can be explained by the availability of NH functions. Indeed, let us recall that for the PDA–IO_4^- coating, acid conditions and a strong oxidant were used to generate the PDA film, generating a different hyperoxidized structure compared to the PDA–O_2 film, with a higher proportion of tertiary amine functions, which does not allow for their chlorination. For the PDA–PEI coating, this drop in N–Cl can be due to the fact that NH functions could be engaged in hydrogen bonds with the adjacent catechol functions, which do not allow the chlorination of these amine functions (Figure S5).

Finally, it is possible to obtain the Cl/N ratio in the whole PDA film, not only from the extreme surface, as shown previously by XPS. In order to do that, a chemical dosage using the oxidative properties of the chloramine film is required to follow the oxidation of TNB into the corresponding dimer DTNB, accompanied by a change in color of the solution (Figure S6). Thus, by measuring the optical density at 412 nm, the amount of Cl(+I) immobilized in the PDA film can be determined. The results are reported in Table 3, together with the density of chlorine atoms for each film. The film with the highest density of Cl(+I), hence N–Cl groups, is the PDA–PEI film. Nonetheless, all three films of PDA exhibit a high amount of chlorine, ranging from 5×10^{20} to almost 10^{22} at $\cdot cm^{-3}$.

Table 3. TNB solution absorption (A) at 412 nm after 24 h of immersion of various samples, the number of chlorine atoms, density (Equation (3) of chloramine in PDA–O_2, PDA–IO_4^- and PDA–PEI coatings estimated by TNB dosage, and the Cl_{200}/N atomic ratio considering a N density of 5.3×10^{21} at cm^{-3}.

	A at 412 nm	Cl (at.)	d_{Cl} (at cm^{-3})	Cl_{200}/N
PD—O_2–Cl	0.30	4.0×10^{16}	2.5×10^{21}	0.47
PDA–IO_4^-–Cl	0.50	5.8×10^{15}	5.0×10^{20}	0.10
PDA–PEI–Cl	0.20	9.25×10^{16}	9.25×10^{21}	0.29

This clear difference between the XPS results and the chemical assay with TNB comes first of all from the fact that a quantification technique is used here, which probes the depth of the layer, unlike the XPS analysis, which only gives information on the coating surface. In addition, the nature of the reagent used and the nature of the PDA–IO_4^- coating, which are rougher and denser than the PDA–O_2 coatings (Figure S3), can explain this difference. Indeed, TNB being a bulky molecule makes its infiltration over the entire thickness of the coatings difficult.

3.3. Antibacterial Properties of Chlorinated PDA Surfaces

Several microbiological tests have been performed in order to evaluate the different antibacterial activities of the chlorinated PDA coatings. These tests were performed with *E. coli* ATCC 25922 and *S. epidermidis* CIP 6821. They were carried out following two routes, as follows: a direct route by optical microscopy, using fluorescent stains to evaluate the bacterial adherence and the cell mortality; a second indirect route was based on the recovery of adhered bacteria and viable cell culture counting on agar plates.

The first test was carried out in order to evaluate the adhesive properties of PDA–XX and PDA–XX–Cl coatings towards bacterial suspensions; the main results are presented in Figure 6. The total adhered flora was evaluated by counting the green bacteria present on the surface, after recording several areas on the different surfaces; this green fluorescence was obtained by marking bacteria with SYTO^{TM} 9 fluorescent staining, which penetrates all living and damaged bacteria. The numbering of adhered bacteria was performed using ImageJ software. Looking first at the results for *E. coli* (Figure 6a), one can notice that all the chlorinated surfaces exhibited a decrease in the number of bacteria compared to the respective non-chlorinated surfaces. Hence, for PDA–O_2 and PDA–IO_4^-, the net decrease in bacterial adherence is 25% and 38%, respectively, with significant statistical differences ($p < 0.01$), as shown in Figure S7. Concerning the PDA–PEI surface, a decrease of 21% is observed (Figure 6a), but with no significant difference ($p > 0.01$) (Figure S7). Surprisingly, no such tendencies were observed for the *S. epidermidis* bacterial strain (Figure 6b). The adherence recorded shows no statistically significant differences, meaning that the chlorine substitution does not affect the contact between the surface and the bacterial membrane. This can most likely be explained by the composition of the membrane of Gram-positive bacteria compared to the composition of the membrane of Gram-negative bacteria, with the absence of charged liposaccharides in the membrane in the latter case. In addition, only one relevant statistical difference was observed in the case of the PDA–PEI surface, which exhibited much lower adherence compared to its chlorinated counterpart, with 36% less adhered bacteria. This could, again, be explained by the specific positive charges present on the outer membrane of the Gram-positive bacteria, resulting in charged repulsion between this membrane and the positively charged amine groups of the PEI film under physiological conditions [53].

Following the evaluation of total adherence properties, by recoding green fluorescent bacteria on the various surfaces, a second fluorescent staining was introduced into the system, and microscopy images were recorded again. This second fluorescent stain, propidium iodide, only penetrates damaged bacterial membranes, and, thus, allows us to evaluate the killing properties of a surface using Equation (5).

The results are presented in Figure 6 (red bars above green bars) for the six studied surfaces, and for both Gram-negative and -positive bacterial strains, presenting the number of red bacteria recorded compared to the number of green bacteria recorded on the same surface. For each surface, the percentage of killing is also indicated on the charts. First of all, one can notice the very low killing efficiency obtained with this technique for all the surfaces, with less than 1% of killing on average for all the PDA coatings towards *S. epidermidis* (Figure 6b), and a killing efficiency between 2 and 11% towards *E. coli* (Figure 6a). It is also important to notice that with this live/dead fluorescent technique, one can evaluate the killing properties of surfaces without the bactericidal molecules; for instance, the fact that a PDA–PEI surface exhibits a 4% killing property towards *E. coli* bacteria, compared with the

11% obtained once the PDA–PEI coatings have been chlorinated (Figure 6a). These results may be surprising when compared with those reported in the literature; for instance, with PDA¬–PEI–Cl coating, Chien et al. have shown 99.99% of killing towards *S. aureus* and 99.9% towards *E. coli*, but these results were obtained using an indirect method, ca. CFU numbering on agar plates [34].

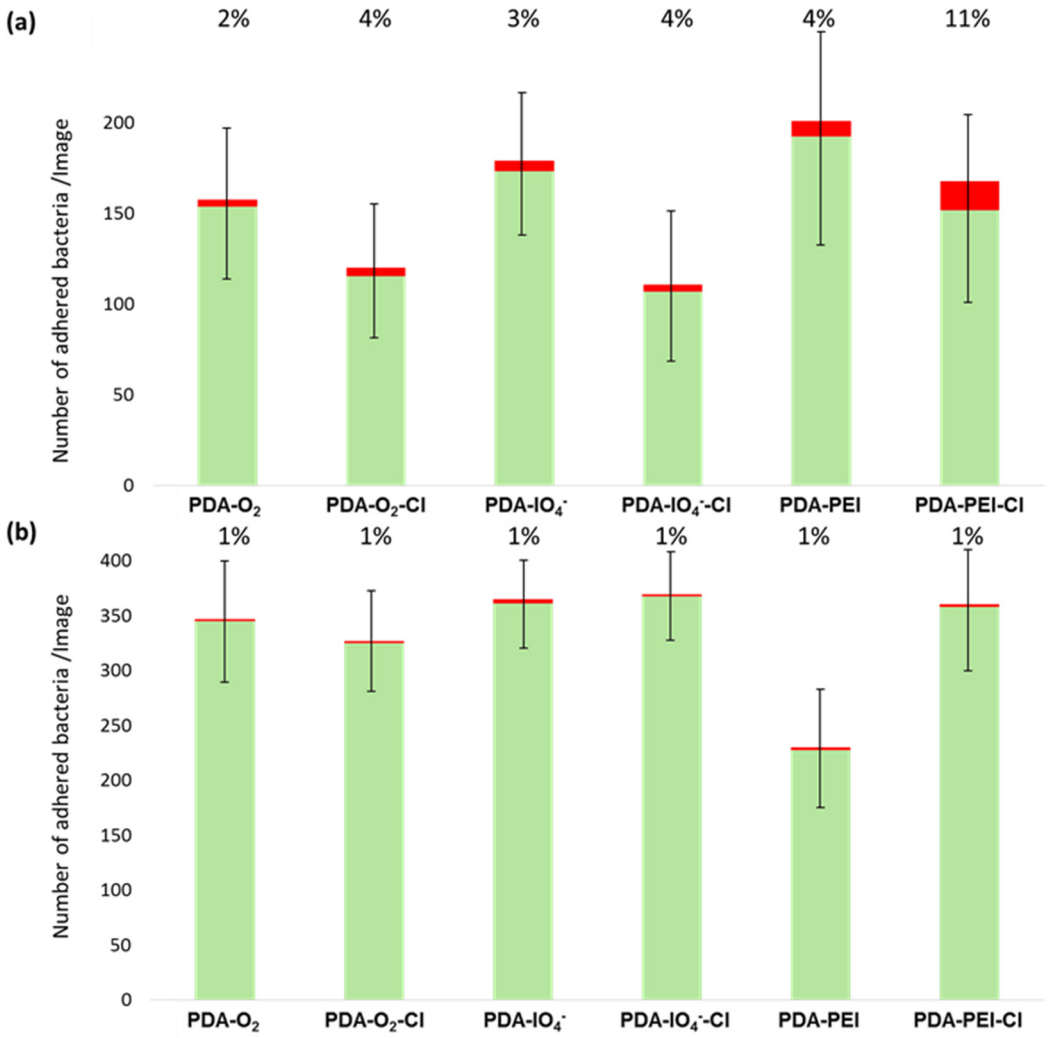

Figure 6. Mean number of adhered bacteria observed by optical microscopy (green bars) and % killing obtained from fluorescence optical microscopy (red bars) for (**a**) *E. coli* and (**b**) *S. epidermidis* and for the three PDA coatings before and after chlorination.

However, it is also known from the literature that live/dead fluorescent techniques are very efficient when the damage caused to the bacteria by the antibacterial agents directly affects the integrity of the membranes of the bacteria. In addition, the mode of actions of haloamines moieties remain unclear and seem to be more directed towards growth inhibition by the blocking of the cellular division, rather than membrane disruption, which could explain the poor number of red bacteria in our fluorescent optical microscopy experiments. Indeed, the contact-active antibacterial mechanism inactivates the growth of the bacteria by remaining bound to surfaces. The mechanism involves the direct transfer of an oxidizing halogen from *N*-halamine to bacterial cells. Halogen has a strong tendency to combine with another element, inhibiting the priming process of bacterial cells. In this way, the antibacterial action occurs without the dissociation of the halogen from haloamine bonds [54].

In addition, we noticed, during our experiments, that the fluorescence intensity varied significantly when passing from the PDA coatings to the chlorinated coatings, without any experimental condition changes. Therefore, we carried out statistical analyses on the size of the bacteria, determined by the average number of pixels observed for each single bacterium. The data are presented in Figure 7. It is quite clear that on non-chlorinated surfaces, the size distribution of adhered bacteria is often observed with a Poisson distribution profile, with a clear apex observed. However, when looking at the shape of this distribution for the chlorinated films, it is clear that the size distribution has changed, with no more Poisson distribution profiles and a net decrease in the size of the bacteria. This size decrease was also observed by scanning electron microscopy (Figure 8). The average size of *E. coli* is around 1.5–1.9 µm for PDA–O_2 films, while the average size is closer to 0.8–1.2 µm when the film has been chlorinated. Moreover, the shape of the bacteria is also affected; it is no longer a clear elongated bacillus shape, but rather an oval shape.

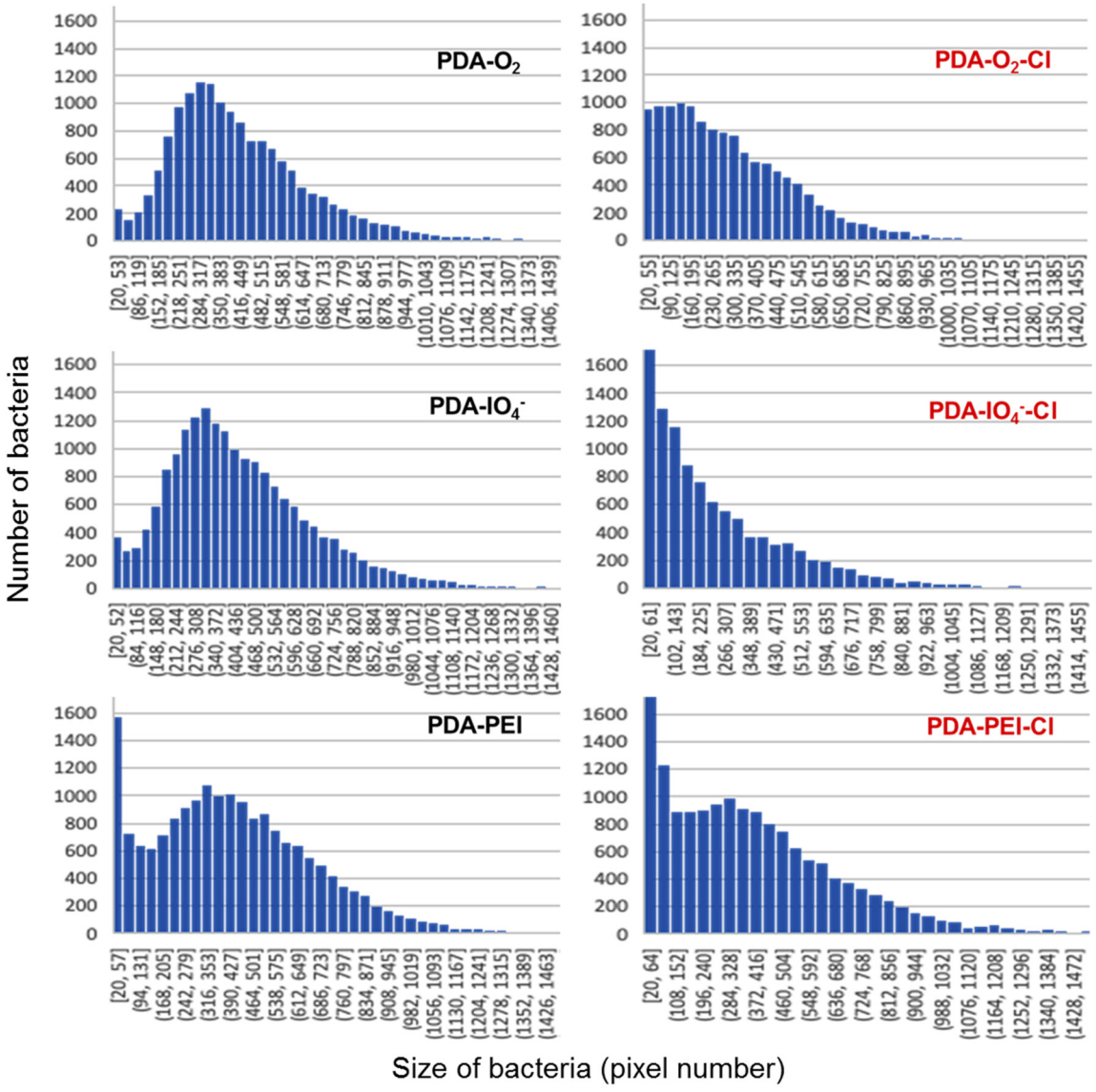

Figure 7. Size distribution (in pixels) of adhered *E. coli* on PDA–X and PDA–X–Cl coatings, observed by optical microscopy with green epifluorescence staining (SYTO^{TM} 9).

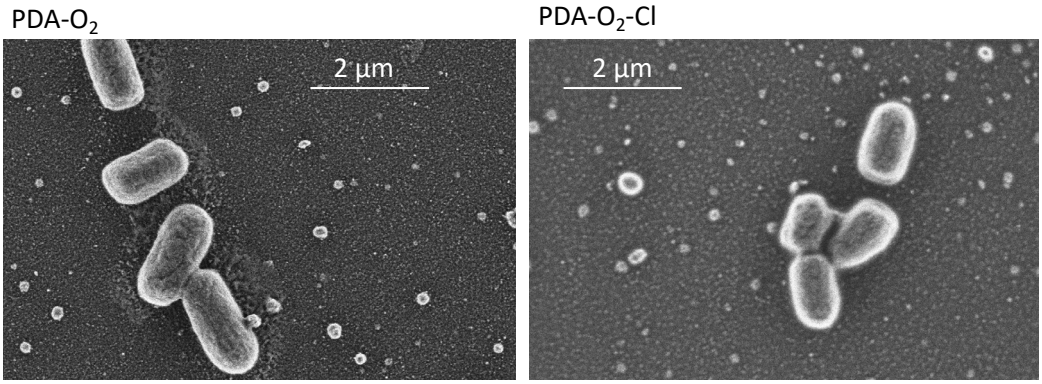

Figure 8. SEM micrographs of *E. coli* on PDA–O_2 (**left**) and PDA–O_2–Cl (**right**) coatings.

The following experiments were carried out using an indirect method, which consisted of recovering adhered bacteria from a given surface (either by mild sonication or by vortexing), in order to count the number of viable bacteria, after the deposition/growth of recovered bacteria on agar plates. The data obtained on agar plates are shown in Figure S8 and Table S1; the results are summarized in Table 4. For each chlorinated surface, two references were used to calculate the *%killing*, either the initial concentration of the bacterial inoculum or by taking into account the respective non-chlorinated surface, using Equation (4).

Table 4. Killing percentage *(%killing)* of chlorinated coating obtained from CFU numbering on agar plates referenced towards the bacterial inoculum and towards the non-chlorinated coatings.

	PDA–Cl		**PDA–IO_4^--Cl**		**PDA–PEI–Cl**	
Reference	**Inoculum**	**PDA**	**Inoculum**	**PDA–IO_4^-**	**Inoculum**	**PDA–PEI**
E. coli ATCC 25922	99.0	34.0	97.7	91.4	97.4	86.2
S. epidermidis CIP 6821	70.0	59.4	83.0	76.6	66.6	58.7

When looking at the results obtained for *E. coli*, and when comparing these to the initial bacterial inoculum, all three PDA-chlorinated surfaces enabled inactivation of bacterial viability close to a 2 log reduction, with the values ranging from 97.4% to 99.0%, as already observed for PDA–O_2 in our previous study [26]. When comparing the PDA-chlorinated surfaces obtained now with the non-chlorinated surface, these *%killing* vary quite significantly as a function of the considered surface. In fact, for the classical PDA–O_2–Cl, the *%killing* is only 34%, while both PDA–IO_4^--Cl and PDA–PEI–Cl exhibit *%killing* higher than 86%. In the case of PDA–IO_4^--Cl, this difference can be explained by the fact that the film is thicker. However, at this point, it should be noted that I atoms could also participate in the antibacterial properties of this PDA film. In the case of PDA–PEI, this can be explained by the fact that more NH groups are available for chlorination (see XPS data in Tables 1 and 2), with more N–Cl functions available overall.

The tendencies are more or less the same when looking at the data obtained for *S. epidermidis*, with higher *%killing* of the chlorinated films when referenced to the inoculum than when referenced to the non-chlorinated coatings. However, lower killing efficiencies are observed towards *S. epidermidis* incomparison to those observed for *E. coli*. This could be explained by the composition of the bacterial membrane of Gram-positive bacteria, as already observed by Targosz et al. [55], with an enriched peptidoglycan concentration for Gram-positive bacteria. Nonetheless, this coating seems to have better efficiency than the other two. Further experiments should be conducted to specify the role of the iodine atoms immobilized on/in the PDA coating of PDA–IO_4^--Cl.

4. Discussion

In this work, we studied the optimization of the antibacterial response of *N*-halamine coatings based on PDA film. A previous study demonstrated the elaboration of a new antibacterial coating formed by a thin chlorinated PDA film, containing chloramine functions inside the polymer. The amount of these functions was estimated to be between 10^{21} and 10^{22} at cm^{-3} [26], giving, for chlorinated PDA coatings, an *E. coli* adhesion reduction of up to 45%, compared to the uncoated surfaces, and a bacterial viability reduction of 99% on the chlorinated PDA coating compared to the initial inoculum concentration, and 34% when compared to the non-chlorinated PDA film.

In order to optimize the amount of haloamine functions available on/in the material to be protected, we have studied other PDA deposition pathways, in order to increase the amount of amine functions immobilized on the surface. For this, two additional routes were considered. The first route was to accelerate the kinetics of PDA film formation by using a more powerful oxidant, ca. sodium periodate, and increase the thickness of the deposit that reaches 100 nm after 24 h. However, the PDA coating is rough and iodine atoms remain trapped on/in the coating. The second route consisted of the use of a second polymer, richer in amine functions, PEI. PEI is known to act as a crosslinker within the structure of PDA, thus allowing more stable coatings to be obtained. The PM-RAIRS analyses confirmed the deposition of the composite, and the XPS measurements have shown enrichment of the PDA–PEI coating in amine functions.

Chlorination of the different PDA films was carried out using diluted NaOCl as a function of contact time and concentration, in order to optimize the chlorination process. According to the XPS analysis, probing the extreme film surface, we have concluded that the efficiency of chlorination was the best for the PDA–O_2 films, with more than 60% of the N atoms being chlorinated, while this value is only 30% for the other two films. These differences between the PDA–O_2, PDA–IO_4^- and PDA–PEI coatings can be explained by the availability of NH functions. Indeed, the PDA–IO_4^- coating is composed of different hyperoxidized structures compared to the PDA–O_2 film, with a higher proportion of tertiary amine functions for which no chlorination is possible. For the PDA–PEI coating, NH_2 functions can be engaged in hydrogen bonds with the adjacent catechol functions, which do not allow chlorination. The chlorination quantification of all of the films was carried out by chemical assay with TNB, and revealed that the PDA–PEI film shows the highest density of N–Cl groups, even though it is not the film that has the higher N/Cl ratio. The three films of PDA exhibit a high amount of chlorine, ranging from 5×10^{20} to almost 10^{22} atoms per cm^3. We noticed a difference between the XPS results and chemical assay with TNB, due, first of all, to the fact that a quantification technique was used here, which probes the depth of the film, unlike the XPS analysis, which only provides information on the film surface. Moreover, due to the nature of the PDA–IO_4^- coating, which is rougher and denser than the PDA–O_2 coating, diffusion of TNB molecules through the entire thickness of the coating could be difficult.

Then, the efficiency of the non-chlorinated and chlorinated coatings in eliminating the following two bacterial strains was studied: one Gram-positive bacteria, *Staphylococcus epidermidis* CIP 6821, and one Gram-negative bacteria, *Escherichia coli* ATCC 25922. The first test was carried out following a direct experiment by optical microscopy, using fluorescent stains to evaluate bacterial adherence and cell mortality. For *E. coli*, all the chlorinated surfaces exhibited a lower number of bacteria compared to the respective non-chlorinated surfaces. For PDA–O_2 and PDA–IO_4^-, the net decrease in bacterial adherence was 25% and 38%, respectively. Concerning the PDA–PEI surface, a decrease of 21% was observed, but with no significant difference ($p > 0.01$). Surprisingly, for the *S. epidermidis* bacterial strain, all the adherence values recorded showed no statistically significant difference. This finding could be explained by the composition of the membrane of Gram-positive bacteria, with the presence of charged liposaccharides and peptidoglycans [55]. Moreover, the PDA–PEI surface exhibited much lower adherence, with 36% less adhered bacteria compared to the chlorinated film. This result could be due, again, to the positive charges present on the

outer membrane of *S. epidermidis* bacteria, resulting in charged repulsion between these charges and the positively charged amine groups of PEI.

Following the evaluation of adherence properties, the killing properties of the PDA films were evaluated. A poor killing efficiency was obtained with this technique for all of the tested PDA surfaces. We can notice that the live/dead fluorescent technique is very efficient when the damage caused to the bacteria by the antibacterial agents directly affects the integrity of the bacterial membrane. Thus, the mode of actions of haloamine moieties seems to be more directed towards growth inhibition, by blocking the cellular division, rather than membrane disruption, which could explain the poor number of red bacteria observed during our fluorescent optical microscopy experiments. This was confirmed by a statistical analysis of the size of the bacteria grown on chlorinated film; looking at the shape of this distribution (Figure 7), it is clear that the bacteria size changed, with a net increase in the number of small bacteria. In fact, the average size of *E. coli* that adhered to the chlorinated PDA film was one-third smaller than the size of the bacteria that adhered to the un-chlorinated PDA film. Moreover, the shape of the bacteria was also affected, becoming an oval shape (Figure 8).

A second indirect route was based on the recovery of adhered bacteria and viable cell culture counting on agar plates. When looking at the results obtained for *E. coli*, and when comparing to the initial bacterial inoculum, it can be observed that the three chlorinated PDA surfaces enable inactivation of bacterial viability, close to a 2 log reduction, with the values ranging from 97.4% to 99.0%, as already observed for the PDA–O_2 film in our previous study [26]. However, when comparing this with the non-chlorinated surface, for the classical PDA–O_2–Cl film, the *%killing* is only 34%, while the PDA–IO_4^--Cl and PDA–PEI–Cl films exhibit *%killing* higher than 86%. These differences could be explained in the case of PDA–IO_4^--Cl, by a thicker and more dense film (Figures S2 and S3), rendering the haloamine functions more accessible for antibacterial activity. In the case of PDA–PEI, it can be explained by the fact that more NH groups are available for chlorination, with more overall N–Cl functions available. The tendencies were quite similar for *S. epidermidis*, with a higher *%killing* of the chlorinated films, when referenced to the inoculum, rather than when referenced to the non-chlorinated coatings. However, lower killing efficiencies were observed towards *S. epidermidis* compared to those for *E. coli*, and that could, again, be explained by the composition of the bacterial membrane.

5. Conclusions

To conclude, in this study, we have shown how to elaborate several PDA-based antibacterial coatings composed of thin *N*-halamine films. Three routes have been followed. First, a "classical" route, with PDA formed with TRIS in the presence of atmospheric O_2. A second route was obtained by changing the oxidizing agent, by replacing the atmospheric O_2 with a stronger oxidant agent, $NaIO_4$. Finally, a copolymer PDA–PEI, using the conditions of the "classical" route, was used. The three coatings exhibit similar haloamine concentrations in the order of 2.5×10^{21} and 9×10^{21} Cl at·cm^{-3} for PDA–O_2 and PDA–PEI, respectively. It is noteworthy that for the PDA–IO_4^- coatings, the Cl(+I) density is four times lower. Microbiological tests were carried out on two bacterial strains, *E. coli* and *S. epidermidis*. Direct tests and fluorescent staining observed by optical microscopy have revealed a clear decrease in bacterial adherence for *E. coli*, up to 40%, while no statistical decrease was observed for *S. epidermidis*. In addition, these direct tests have shown that the morphology of the bacteria after contact with the *N*-halamine coating has changed, with a smaller size and distorted shape. Indirect tests evidenced differences in the viability/growth of adhered bacteria, with bactericidal properties higher in the case of Gram-negative bacteria than for Gram-positive bacteria. The reduction in viable bacteria is higher when compared to the initial inoculum, rather than when compared to the non-chlorinated surfaces. Finally, for both bacterial strains, the best PDA coating appears to be the PDA–IO_4^--Cl coating, especially when considering that it contains four times less active haloamine functions for a 25% better bactericidal efficiency.

Supplementary Materials: The following supporting information can be downloaded at: https://www.mdpi.com/article/10.3390/colloids6010009/s1: Figure S1. PM-RAIRS spectra of gold surfaces coated with PDA–O_2, PDA–IO_4^- and PDA–PEI films. Figure S2. PDA–O2, PDA–IO4− and PDA–PEI film thickness evaluated by SEM observations and ellipsometry measurements. Figure S3. SEM micrographs of PDA–O2, PDA–IO4− and PDA–PEI coatings on gold substrates. Figure S4. Evolution of the contact angle with water for PDA–O2, PDA–IO4− and PDA–PEI coatings. Figure S5. Representative structural components in PDA–IO4− and PDA–PEI films. Figure S6. Numbering of chloramine functions by TNB. Figure S7. Statistical analyses of bacterial adherence. Figure S8. Optical photographs of agar plates presenting the killing tests results. Table S1. Average number of bacteria, in CFU mL^{-1}, after killing tests against the different PDA coatings.

Author Contributions: Conceptualization, C.D.-C. and V.H.; methodology, C.D.-C. and V.H.; validation, C.D.-C. and V.H.; formal analysis, N.N. and A.M.; investigation, N.N. and A.M.; writing—original draft preparation, N.N., A.M., C.D.-C. and V.H.; writing—review and editing, N.N., A.M., C.D.-C. and V.H.; supervision, C.D.-C. and V.H.; funding acquisition, C.D.-C. and V.H. All authors have read and agreed to the published version of the manuscript.

Funding: A.M. would like to thank the European cross-border cooperation program Interreg Franco-Suisse 2014–2020 and the FEDER agency (Fonds Européen de Développement Régional) for funding. This work was also supported by French state funds, managed by the ANR within the Investissements d'Avenir program, under reference ANR-11-IDEX-0004-02, and more specifically within the framework of the Cluster of Excellence MATISSE, which provided experimental support funding for N.N. This work was partly supported by the French Renatech network and its FEMTO-ST technological facility (SEM-FEG Imaging).

Institutional Review Board Statement: Not applicable.

Informed Consent Statement: Not applicable.

Data Availability Statement: The data presented in this study are available on request from the correspondings authors.

Acknowledgments: The authors acknowledge IMPC (Institut des Matériaux de Paris Centre, FR2482) and the C'Nano project of Region Ile-de-France, for Omicron XPS apparatus funding. A.M and V.H. would like to thank Marina Raschetti for her help in setting up the experiments with SEM-FEG.

Conflicts of Interest: The authors declare no conflict of interest.

References

1. de Carvalho, C.C.C.R. Marine Biofilms: A Successful Microbial Strategy with Economic Implications. *Front. Mar. Sci.* **2018**, *5*, 126. [CrossRef]
2. Hall-Stoodley, L.; Costerton, J.W.; Stoodley, P. Bacterial Biofilms: From the Natural Environment to Infectious Diseases. *Nat. Rev. Microbiol.* **2004**, *2*, 95–108. [CrossRef] [PubMed]
3. Nickel, J.C.; Ruseska, I.; Wright, J.B.; Costerton, J.W. Tobramycin Resistance of Pseudomonas Aeruginosa Cells Growing as a Biofilm on Urinary Catheter Material. *Antimicrob. Agents Chemother.* **1985**, *27*, 619–624. [CrossRef] [PubMed]
4. Rabin, N.; Zheng, Y.; Opoku-Temeng, C.; Du, Y.; Bonsu, E.; Sintim, H.O. Biofilm Formation Mechanisms and Targets for Developing Antibiofilm Agents. *Future Med. Chem.* **2015**, *7*, 493–512. [CrossRef]
5. Veerachamy, S.; Yarlagadda, T.; Manivasagam, G.; Yarlagadda, P.K. Bacterial Adherence and Biofilm Formation on Medical Implants: A Review. *Proc. Inst. Mech. Eng. H* **2014**, *228*, 1083–1099. [CrossRef]
6. Donlan, R.M. Biofilms: Microbial Life on Surfaces. *Emerg. Infect. Dis.* **2002**, *8*, 881–890. [CrossRef]
7. Dufour, D.; Leung, V.; Lévesque, C.M. Bacterial Biofilm: Structure, Function, and Antimicrobial Resistance. *Endod. Top.* **2010**, *22*, 2–16. [CrossRef]
8. Alves, D.; Pereira, M.O. Mini-Review: Antimicrobial Peptides and Enzymes as Promising Candidates to Functionalize Biomaterial Surfaces. *Biofouling* **2014**, *30*, 483–499. [CrossRef]
9. Chen, J.; Zhu, Y.; Xiong, M.; Hu, G.; Zhan, J.; Li, T.; Wang, L.; Wang, Y. Antimicrobial Titanium Surface via Click-Immobilization of Peptide and Its in Vitro/Vivo Activity. *ACS Biomater. Sci. Eng.* **2019**, *5*, 1034–1044. [CrossRef]
10. Cox, H.J.; Li, J.; Saini, P.; Paterson, J.R.; Sharples, G.J.; Badyal, J.P.S. Bioinspired and Eco-Friendly High Efficacy Cinnamaldehyde Antibacterial Surfaces. *J. Mater. Chem. B* **2021**, *9*, 2918–2930. [CrossRef]
11. Nicolas, M.; Beito, B.; Oliveira, M.; Tudela Martins, M.; Gallas, B.; Salmain, M.; Boujday, S.; Humblot, V. Strategies for Antimicrobial Peptides Immobilization on Surfaces to Prevent Biofilm Growth on Biomedical Devices. *Antibiotics* **2022**, *11*, 13. [CrossRef] [PubMed]

12. Shahnawaz Khan, M.; Abdelhamid, H.N.; Wu, H.-F. Near Infrared (NIR) Laser Mediated Surface Activation of Graphene Oxide Nanoflakes for Efficient Antibacterial, Antifungal and Wound Healing Treatment. *Colloids Surf. B Biointerfaces* **2015**, *127*, 281–291. [CrossRef] [PubMed]
13. Siedenbiedel, F.; Tiller, J. Antimicrobial Polymers in Solution and on Surfaces: Overview and Functional Principles. *Polymers* **2012**, *4*, 46–71. [CrossRef]
14. Fan, X.; Ren, X.; Huang, T.-S.; Sun, Y. Cytocompatible Antibacterial Fibrous Membranes Based on Poly(3-Hydroxybutyrate-Co-4-Hydroxybutyrate) and Quaternarized N-Halamine Polymer. *RSC Adv.* **2016**, *6*, 42600–42610. [CrossRef]
15. Kügler, R.; Bouloussa, O.; Rondelez, F. Evidence of a Charge-Density Threshold for Optimum Efficiency of Biocidal Cationic Surfaces. *Microbiology* **2005**, *151*, 1341–1348. [CrossRef] [PubMed]
16. Olsen, I. Biofilm-Specific Antibiotic Tolerance and Resistance. *Eur. J. Clin. Microbiol. Infect. Dis.* **2015**, *34*, 877–886. [CrossRef]
17. Olson, M.E.; Ceri, H.; Morck, D.W.; Buret, A.G.; Read, R.R. Biofilm Bacteria: Formation and Comparative Susceptibility to Antibiotics. *Can. J. Vet. Res.* **2002**, *66*, 86–92.
18. Timofeeva, L.; Kleshcheva, N. Antimicrobial Polymers: Mechanism of Action, Factors of Activity, and Applications. *Appl. Microbiol. Biotechnol.* **2011**, *89*, 475–492. [CrossRef]
19. Baltzer, S.A.; Brown, M.H. Antimicrobial Peptides: Promising Alternatives to Conventional Antibiotics. *J. Mol. Microbiol. Biotechnol.* **2011**, *20*, 228–235. [CrossRef]
20. Bang, S.H.; Sekhon, S.S.; Ahn, J.-Y.; Kim, Y.-H.; Min, J. Advances in Antimicrobial Agents Based Lysosomes. *Mol. Cell Toxicol.* **2014**, *10*, 229–235. [CrossRef]
21. Bechinger, B.; Gorr, S.U. Antimicrobial Peptides: Mechanisms of Action and Resistance. *J. Dent. Res.* **2017**, *96*, 254–260. [CrossRef] [PubMed]
22. Harris, F.; Dennison, S.R.; Phoenix, D.A. Anionic Antimicrobial Peptides from Eukaryotic Organisms. *Curr. Protein Pept. Sci.* **2009**, *10*, 585–606. [CrossRef] [PubMed]
23. Shima, S.; Matsuoka, H.; Iwamoto, T.; Sakai, H. Antimicrobial Action of Epsilon-Poly-L-Lysine. *J. Antibiot.* **1984**, *37*, 1449–1455. [CrossRef] [PubMed]
24. Dong, A.; Wang, Y.-J.; Gao, Y.; Gao, T.; Gao, G. Chemical Insights into Antibacterial N-Halamines. *Chem. Rev.* **2017**, *117*, 4806–4862. [CrossRef]
25. Hui, F.; Debiemme-Chouvy, C. Antimicrobial N-Halamine Polymers and Coatings: A Review of Their Synthesis, Characterization, and Applications. *Biomacromolecules* **2013**, *14*, 585–601. [CrossRef]
26. Nazi, N.; Humblot, V.; Debiemme-Chouvy, C. A New Antibacterial N-Halamine Coating Based on Polydopamine. *Langmuir* **2020**, *36*, 11005–11014. [CrossRef]
27. Chien, H.-W.; Chiu, T.-H. Stable N-Halamine on Polydopamine Coating for High Antimicrobial Efficiency. *Eur. Polym. J.* **2020**, *130*, 109654. [CrossRef]
28. Liu, Y.; Ai, K.; Lu, L. Polydopamine and Its Derivative Materials: Synthesis and Promising Applications in Energy, Environmental, and Biomedical Fields. *Chem. Rev.* **2014**, *114*, 5057–5115. [CrossRef]
29. Ye, Q.; Zhou, F.; Liu, W. Bioinspired Catecholic Chemistry for Surface Modification. *Chem. Soc. Rev.* **2011**, *40*, 4244–4258. [CrossRef]
30. Ball, V. Physicochemical Perspective on "Polydopamine" and "Poly(Catecholamine)" Films for Their Applications in Biomaterial Coatings. *Biointerphases* **2014**, *9*, 030801. [CrossRef]
31. Ponzio, F.; Ball, V. Polydopamine Deposition at Fluid Interfaces. *Polym. Int.* **2016**, *65*, 1251–1257. [CrossRef]
32. Ponzio, F.; Barthès, J.; Bour, J.; Michel, M.; Bertani, P.; Hemmerlé, J.; d'Ischia, M.; Ball, V. Oxidant Control of Polydopamine Surface Chemistry in Acids: A Mechanism-Based Entry to Superhydrophilic-Superoleophobic Coatings. *Chem. Mater.* **2016**, *28*, 4697–4705. [CrossRef]
33. Lv, Y.; Yang, S.-J.; Du, Y.; Yang, H.-C.; Xu, Z.-K. Co-Deposition Kinetics of Polydopamine/Polyethyleneimine Coatings: Effects of Solution Composition and Substrate Surface. *Langmuir* **2018**, *34*, 13123–13131. [CrossRef]
34. Chien, H.W.; Chiu, T.H.; Lee, Y.L. Rapid Biocidal Activity of N-Halamine-Functionalized Polydopamine and Polyethylene Imine Coatings. *Langmuir* **2021**, *37*, 8037–8044. [CrossRef]
35. Humblot, V.; Yala, J.-F.; Thebault, P.; Boukerma, K.; Hequet, A.; Berjeaud, J.-M.; Pradier, C.-M. The Antibacterial Activity of Magainin I Immobilized onto Mixed Thiols Self-Assembled Monolayers. *Biomaterials* **2009**, *30*, 3503–3512. [CrossRef]
36. Lee, B.P.; Messersmith, P.B.; Israelachvili, J.N.; Waite, J.H. Mussel-Inspired Adhesives and Coatings. *Annu Rev. Mater. Res.* **2011**, *41*, 99–132. [CrossRef]
37. Lee, H.; Dellatore, S.M.; Miller, W.M.; Messersmith, P.B. Mussel-Inspired Surface Chemistry for Multifunctional Coatings. *Science* **2007**, *318*, 426–430. [CrossRef]
38. Del Frari, D.; Bour, J.; Ball, V.; Toniazzo, V.; Ruch, D. Degradation of Polydopamine Coatings by Sodium Hypochlorite: A Process Depending on the Substrate and the Film Synthesis Method. *Polym. Degrad. Stab.* **2012**, *97*, 1844–1849. [CrossRef]
39. Ma, K.; Jiang, Z.; Li, L.; Liu, Y.; Ren, X.; Huang, T.-S. N-Halamine Modified Polyester Fabrics: Preparation and Biocidal Functions. *Fibers Polym.* **2014**, *15*, 2340–2344. [CrossRef]
40. Scofield, J.H. Hartree-Slater Subshell Photoionization Cross-Sections at 1254 and 1487 eV. *J. Electron Spectrosc. Relat. Phenom.* **1976**, *8*, 129–137. [CrossRef]

41. Riddles, P.W.; Blakeley, R.L.; Zerner, B. Ellman's Reagent: 5,5′-Dithiobis(2-Nitrobenzoic Acid) a Reexamination. *Anal. Biochem.* **1979**, *94*, 75–81. [CrossRef]
42. Debiemme-Chouvy, C.; Haskouri, S.; Folcher, G.; Cachet, H. An Original Route to Immobilize an Organic Biocide onto a Transparent Tin Dioxide Electrode. *Langmuir* **2007**, *23*, 3873–3879. [CrossRef]
43. Segut, O.; Herlem, G.; Lakard, B.; Blondeau-Patissier, V.; Nardin, M.; Gree, S.; Rauch, J.-Y. Electrochemically Deposited Polyethyleneimine Films and Their Characterization. *Synth. Met.* **2010**, *160*, 1359–1364. [CrossRef]
44. Zangmeister, R.A.; Morris, T.A.; Tarlov, M.J. Characterization of Polydopamine Thin Films Deposited at Short Times by Autoxidation of Dopamine. *Langmuir* **2013**, *29*, 8619–8628. [CrossRef]
45. Chen, T.-P.; Liu, T.; Su, T.-L.; Liang, J. Self-Polymerization of Dopamine in Acidic Environments without Oxygen. *Langmuir* **2017**, *33*, 5863–5871. [CrossRef]
46. Jiang, J.; Zhu, L.; Zhu, L.; Zhu, B.; Xu, Y. Surface Characteristics of a Self-Polymerized Dopamine Coating Deposited on Hydrophobic Polymer Films. *Langmuir* **2011**, *27*, 14180–14187. [CrossRef]
47. Zheng, W.; Fan, H.; Wang, L.; Jin, Z. Oxidative Self-Polymerization of Dopamine in an Acidic Environment. *Langmuir* **2015**, *31*, 11671–11677. [CrossRef]
48. Weidman, S.W.; Kaiser, E.T. The Mechanism of the Periodate Oxidation of Aromatic Systems. III. A Kinetic Study of the Periodate Oxidation of Catechol. *J. Am. Chem. Soc.* **1966**, *88*, 5820–5827. [CrossRef]
49. Alfieri, M.L.; Panzella, L.; Oscurato, S.L.; Salvatore, M.; Avolio, R.; Errico, M.E.; Maddalena, P.; Napolitano, A.; D'Ischia, M. The Chemistry of Polydopamine Film Formation: The Amine-Quinone Interplay. *Biomimetics* **2018**, *3*, 26. [CrossRef]
50. Tanuma, S.; Powell, C.J.; Penn, D.R. Calculation of Electron Inelastic Mean Free Paths (IMFPs) VII. Reliability of the TPP-2M IMFP Predictive Equation. *Surf. Interface Anal.* **2003**, *35*, 268–275. [CrossRef]
51. Xu, L.; Zuo, Y.Y. Reversible Phase Transitions in the Phospholipid Monolayer. *Langmuir* **2018**, *34*, 8694–8700. [CrossRef] [PubMed]
52. Yang, W.; Liu, C.; Chen, Y. Stability of Polydopamine Coatings on Gold Substrates Inspected by Surface Plasmon Resonance Imaging. *Langmuir* **2018**, *34*, 3565–3571. [CrossRef] [PubMed]
53. Curtis, K.A.; Miller, D.; Millard, P.; Basu, S.; Horkay, F.; Chandran, P.L. Unusual Salt and pH Induced Changes in Polyethylenimine Solutions. *PLoS ONE* **2016**, *11*, e0158147. [CrossRef] [PubMed]
54. Luo, J.; Chen, Z.; Sun, Y. Controlling Biofilm Formation with an N-Halamine-Based Polymeric Additive. *J. Biomed. Mater. Res.* **2006**, *77A*, 823–831. [CrossRef] [PubMed]
55. Marcinkiewicz, J.; Biedroń, R.; Białecka, A.; Kasprowicz, A.; Mak, M.; Targosz, M. Susceptibility of Propionibacterium Acnes and Staphylococcus Epidermidis to Killing by MPO-Halide System Products. Implication for Taurine Bromamine as a New Candidate for Topical Therapy in Treating Acne Vulgaris. *Arch. Immunol. Ther. Exp.* **2006**, *54*, 61–68. [CrossRef]